Linear Reduced-Order Model of Airfoil Gust Response

Amir K. Bagheri,[1] Dorian P. Jones[2], Ann L. Gaitonde[3]
University of Bristol, Bristol, England BS8 1TR, United Kingdom

Nomenclature

A, B, C, D	=	Continuous state-space matrices
$\hat{A}, \hat{B}, \hat{C}, \hat{D}$	=	Discrete state-space matrices
$\hat{A}_r, \hat{B}_r, \hat{C}_r, \hat{D}_r$	=	Reduced discrete state-space matrices
$\Delta\alpha_{eff}$	=	Effective change in angle of attack
G	=	Discrete-system transfer function
$\widehat{H}$	=	Hankel matrix
k_{red}	=	Reduced frequency
$\mathcal{L}$	=	Lagrangian function
λ	=	Gust length
ω	=	Continuous frequency
$\hat{\omega}$	=	Discrete frequency
s	=	Laplace variable
T	=	Sampling period
$\boldsymbol{u}$	=	Discrete input vector
U_{ref}	=	Reference flow velocity
$v_{g_{max}}$	=	Gust amplitude
$\boldsymbol{x}$	=	State vector
$\boldsymbol{y}$	=	Output vector
z	=	Z-transform variable

[1] Research Associate, Department of Aerospace Engineering, Queen's Building, University Walk.
[2] Reader in Aerodynamics, Department of Aerospace Engineering, Queen's Building, University Walk.
[3] Reader in Aerodynamics, Department of Aerospace Engineering, Queen's Building, University Walk.

I.Introduction

Unsteady gust loads are some of the critical loads an aircraft experiences and thus there is a need for more accurate computational models to predict gust loads at lower cost than high fidelity Computational Fluid Dynamics (CFD). Reduced Order Models (ROMs) have been investigated in CFD, with construction occurring in the discrete time or frequency domain in which codes are implemented. Many ROM methods assume flow linearity such as Eigensystem Realization Algorithm (ERA) [1], [2], Proper Orthogonal Decomposition [3], [4], [5], convolution and Volterra theory [6] and Arnoldi reduction [7]. In recent years there has been a focus on non-linear ROMs [8], [9], [10] with a variety of approaches used.

Only a few studies have focused on gusts. Raveh [11] created ROMs for a wing excited by a gust, using time-domain convolution. Skujins *et al* [9] created ROMs based on linear convolution across Mach regimes, developing a method-of-segments to assist in ROM construction. Gennaretti *et al* [12] compared linear aeroelastic ROMs, based on p-transform, and rational matrix approximation (RMA) of transfer functions, for gust responses of a flexible wing. Wales *et al* [8] created ROMs to predict airfoil gust response using ERA, introducing nonlinearity using nonlinear steady-state data.

Here, ROMs for a rigid airfoil encountering a gust are based on the subspace system identification algorithm methods [13]. The key difference is that here the system is known. The application is one of Model Order Reduction (MOR) rather than identification. The basic method is extended for the first time to ensure ROM stability and to force the ROM steady state response to match exactly the full order model from which it is derived. Unlike common POD methods, the subspace-based MOR method does not require the formation and storage of large matrices. The relationship of the current method to frequency-based POD methods, mirrors that between ERA and time domain snapshot approximate balanced POD.

II.Background

A. Continuous and Discrete Systems

Linearizing the CFD equations yields the continuous state-space system

$$\begin{aligned} \dot{\boldsymbol{x}} &= \boldsymbol{A}\boldsymbol{x} + \boldsymbol{B}\boldsymbol{u} \\ \boldsymbol{y} &= \boldsymbol{C}\boldsymbol{x} + \boldsymbol{D}\boldsymbol{u} \end{aligned} \tag{1}$$

where A, B, C and D are continuous state matrices. Putting these into discrete form yields:

$$\begin{aligned} \boldsymbol{x_d(n+1)} &= \boldsymbol{\hat{A}x_d(n) + \hat{B}u_d(n)} \\ \boldsymbol{y_d(n)} &= \boldsymbol{\hat{C}x_d(n) + \hat{D}u_d(n)} \end{aligned} \tag{2}$$

$\boldsymbol{x_d} \in \mathbb{R}^{n\times 1}$ is a discrete-time state vector; $\boldsymbol{u_d} \in \mathbb{R}^{r\times 1}$ is the time level nT input vector (T is the sampling period); $\boldsymbol{y_d} \in \mathbb{R}^{m\times 1}$ approximates the continuous-system output vector at $t = nT$ and $\hat{A}, \hat{B}, \hat{C}$ and $\hat{D}$ are discrete state matrices. The continuous-time transfer function equals the frequency response of the continuous system if

$$s = j\omega \tag{3}$$

where ω is the continuous-domain frequency and the discrete-time transfer function G equals the frequency response of the discrete system if

$$z = e^{j\hat{\omega}} \tag{4}$$

where $\hat{\omega}$ is the discrete-domain frequency. The discrete and continuous-domain transfer functions are identical if

$$s = \frac{2}{T}\frac{z-1}{z+1} \tag{5}$$

and the discrete and frequency domain solutions correspond if:

$$\omega = \frac{2}{T}\tan\left(\frac{\hat{\omega}}{2}\right) \tag{6}$$

Here, the DLR TAU viscous Linear Frequency Domain (LFD) solver with a Spalart-Allmaras turbulence model is used to obtain continuous frequency-domain solutions. This assumes small amplitude unsteady motion, which restricts the size of gust disturbances that can be modeled. However, linearized methods are adequate for certification gusts and can be corrected using non-linear data to extend applicability [14].

B. Model Order Reduction

Following [13] G_k is obtained at M+1 equi-spaced discrete frequencies $\hat{\omega}_k$ (between 0 and π) by finding ω_k (6) and running the LFD code. The transfer functions are extended to the full unit circle using complex conjugates:

$$G_{M+k} = G^*_{M-k} \qquad k = 1, \ldots, M-1 \tag{7}$$

A Hankel matrix $\hat{H}$ is defined [13]:

$$\hat{H} \stackrel{\text{def}}{=} \begin{bmatrix} \hat{h}_1 & \hat{h}_2 & \cdots & \hat{h}_M \\ \hat{h}_2 & \hat{h}_3 & \cdots & \hat{h}_{M+1} \\ \vdots & \vdots & \ddots & \vdots \\ \hat{h}_M & \hat{h}_{M+1} & \cdots & \hat{h}_{2M-1} \end{bmatrix} \in \mathbb{R}^{M\times M} \tag{8}$$

$$\hat{h}_i \overset{\text{def}}{\equiv} \frac{1}{2M}\sum_{k=0}^{2M-1} G_k e^{\frac{j2\pi ik}{2M}} \qquad i = 0, \ldots, 2M-1 \tag{9}$$

Retaining the *r* largest singular values in a Singular Value Decomposition (SVD) of $\hat{H}$:

$$\hat{H} = [\hat{U}_r \quad \hat{U}_o]\begin{bmatrix}\hat{\Sigma}_r & 0\\ 0 & \hat{\Sigma}_o\end{bmatrix}\begin{bmatrix}\hat{V}_r^T\\ \hat{V}_o^T\end{bmatrix} \tag{10}$$

gives reduced discrete system matrices as:

$$\begin{aligned}\hat{A}_r &= \left(J_1\hat{U}_r\right)^{\dagger} J_2\hat{U}_r\\ \hat{C}_r &= J_3\hat{U}_r\end{aligned} \tag{11}$$

where

$$\begin{aligned}J_1 &= [I_{M-1} \quad 0]_{M-1\times M}\\ J_2 &= [0 \quad I_{M-1}]_{M-1\times M}\\ J_3 &= [I \quad 0_{M-1}]_{1\times M}\end{aligned} \tag{12}$$

and $X^{\dagger} = (X^TX)^{-1}X^T$ is the Moore-Penrose pseudoinverse of *X*. Then $\hat{B}_r$ and $\hat{D}_r$ are

$$\begin{bmatrix}\hat{B}_r\\ \hat{D}_r\end{bmatrix} = \begin{bmatrix}Re\,\hat{\chi}\\ Im\,\hat{\chi}\end{bmatrix}^{\dagger}\begin{bmatrix}Re\,\hat{\mathcal{G}}\\ Im\,\hat{\mathcal{G}}\end{bmatrix} \tag{13}$$

where

$$\hat{\chi} := \begin{bmatrix}\hat{C}_r(e^{j\hat{\omega}_0}I - \hat{A}_r) & I\\ \hat{C}_r(e^{j\hat{\omega}_1}I - \hat{A}_r) & I\\ \vdots & \vdots\\ \hat{C}_r(e^{j\hat{\omega}_M}I - \hat{A}_r) & I\end{bmatrix} \quad , \quad \hat{\mathcal{G}} := \begin{bmatrix}G_0\\ G_1\\ \vdots\\ G_M\end{bmatrix} \tag{14}$$

C. System Stability

A stable discrete reduced system has the eigenvalues of $\hat{A}_r$ inside the unit disk. A McKelvey based ROM can be unstable and hence stabilization methods are developed.

1. Restarting

Restarting is an approach that applies shifts to remove undesirable eigenvalues and identifies a new system [22] and can be performed successively until a stable ROM is found.

Starting from (9), and writing G_l as the Fourier Transform of the system impulse response g_l [15] gives:

$$G_l = \sum_{l=0}^{\infty} g_l e^{-j\hat{\omega}_k l} = \sum_{l=0}^{\infty} g_l e^{\frac{-j\pi kl}{M}} \tag{15}$$

$$\therefore \hat{h}_i = \frac{1}{2M}\sum_{k=0}^{2M-1}\sum_{l=0}^{\infty} g_l e^{\frac{j2\pi k(i-l)}{2M}} = \sum_{l=0}^{\infty} g_i + 2lM = \hat{C}\hat{A}^{i-1}\left(\sum_{l=0}^{\infty}\hat{A}^{2lM}\right)\hat{B}$$
$$= \hat{C}\hat{A}^{i-1}\left(I - \hat{A}^{2M}\right)^{-1}\hat{B} \tag{16}$$

A shift equal to a real unstable eigenvalue, μ_1, is applied to $\hat{C}_r$

$$\overline{\hat{C}_r} = \hat{C}_r(\hat{A}_r - \mu_1 I) \tag{17}$$

Then using (16) with reduced state matrices:

$$\hat{h}_i = \hat{C}_r\left(\hat{A}_r - \mu_1 I\right)\hat{A}_r{}^{i-1}\left(I - \hat{A}_r{}^{2M}\right)^{-1}\hat{B}_r$$
$$= \hat{C}_r\hat{A}_r{}^{i}\left(I - \hat{A}_r{}^{2M}\right)^{-1}\hat{B}_r - \mu_1\hat{C}_r\hat{A}_r{}^{i-1}\left(I - \hat{A}_r{}^{2M}\right)^{-1}\hat{B}_r \tag{18}$$
$$= \hat{h}_{i+1} - \mu_1\hat{h}_i$$

and constructing a new Hankel matrix gives:

$$\widehat{H} = \widehat{H}_{i+1} - \mu_1\widehat{H}_i \tag{19}$$

To remove a complex pair of unstable eigenvalues, a complex pair of shifts is applied to $\hat{C}_r$

$$\overline{\hat{C}_r} = \hat{C}_r(\hat{A}_r - \mu_2 I)(\hat{A}_r - \mu_1 I) \tag{20}$$

which gives the new Hankel matrix:

$$\widehat{H} = \widehat{H}_{i+2} - (\mu_1{+}\mu_2)\widehat{H}_{i+1} + \mu_1\mu_2\widehat{H}_i \tag{21}$$

To construct $\widehat{H}_{i+1}$ or $\widehat{H}_{i+2}$, additional $\hat{h}_i$ are needed. However, here the number of data points is fixed *apriori*, thus each restart requires a reduction in the reduced system size. The ROM method is applied using the new Hankel matrix (19) or (21). This is repeated if the new system is unstable. After restarting, a new $\hat{C}_r$ is constructed:

$$\hat{C}_r = \overline{\hat{C}_r}\left(\prod_{i=1}^{n}\left(\hat{A}_r - \mu_i I\right)^{-1}\right) \tag{22}$$

where *n* is the number of shifts applied. It has been found that typically only 1 or 2 restarts are needed. If significant numbers of restarts were needed, then the number of frequencies used for model creation should be increased.

2. Schur Decomposition

An alternative is Schur decomposition [15], which keeps the magnitude of the frequency response approximately unchanged and has the advantages of needing one step and leaving model size unchanged. However, it was found to be less robust than restarting since it is not physics based, leading to stable but inaccurate ROMs.

First $\hat{A}_r$ is transformed to the complex Schur form with eigenvalues μ_i on the diagonal. Eigenvalues with $1 < |\mu_i| \leq 2$ are projected inside the unit disc: $\mu_i = \mu_i(\frac{2}{|\mu_i|} - 1)$. Eigenvalues with $|\mu_i| > 2$ are set to zero. Eigenvalues on the unit circle are moved by changing the magnitude of the eigenvalue by a small positive ϵ: $\mu_i = \mu_i(1 - \epsilon)$. Finally, the new $\hat{A}_r$ is transformed back to its original form.

D. Steady State Correction

Three methods were considered to correct the zero-frequency response to match the full-order system response. From (13) and (14) the estimated reduced system frequency response is:

$$\hat{\chi}\begin{bmatrix}\hat{B}_r \\ \hat{D}_r\end{bmatrix} = \tilde{G}(z) \tag{23}$$

The product of the first row of the $\hat{\chi}$ matrix with $\begin{bmatrix}\hat{B}_r \\ \hat{D}_r\end{bmatrix}$ gives the zero-frequency response.

1. Adjust $\hat{D}_r$

By shifting $\hat{D}_r$ the entire reduced frequency response is shifted so that the steady state matches the full-order system steady state.

$$\begin{gathered}\hat{\chi}_{1:}\begin{bmatrix}\hat{B}_r \\ \hat{D}_r\end{bmatrix} = \tilde{G}_1 \\ \therefore \overline{\hat{D}_r} = \tilde{G}_1 - \hat{C}_r\left(I - \hat{A}_r\right)^{-1}\hat{B}_r\end{gathered} \tag{24}$$

2. Adjust $\hat{B}_r$

By changing $\hat{B}_r$ by $\hat{B}_\delta$ and minimising $\hat{B}_\delta$ using the Moore-Penrose pseudoinverse the least amount of change required to ensure steady-state matching is found.

$$\begin{gathered}\hat{\chi}_{1:}\begin{bmatrix}\hat{B}_r + \hat{B}_\delta \\ \hat{D}_r\end{bmatrix} = \tilde{G}_1 \\ \therefore [\hat{C}_r(z_0 I - \hat{A}_r)]\hat{B}_\delta = \tilde{G}_1 - \hat{D}_r - [\hat{C}_r(z_0 I - \hat{A}_r)]\hat{B}_r \\ \hat{B}_\delta = [\hat{C}_r(z_0 I - \hat{A}_r)]^\dagger(\tilde{G}_1 - \hat{D}_r - [\hat{C}_r(z_0 I - \hat{A}_r)]\hat{B}_r) \\ \overline{\hat{B}_r} = \hat{B}_r + \hat{B}_\delta\end{gathered} \tag{25}$$

3. Constrained Least Squares

The least squares problem (13) is solved with the constraint that the steady-state response of the reduced system matches that of the full-order system:

$$Minimize \quad \left\| \tilde{G}(z) - \hat{\chi} \begin{bmatrix} \hat{B}_r \\ \hat{D}_r \end{bmatrix} \right\|^2 \quad such\ that \quad \hat{\chi}_{1:} \begin{bmatrix} \hat{B}_r \\ \hat{D}_r \end{bmatrix} = \tilde{G}_1 \tag{26}$$

This is solved by forming a Lagrangian Function, with Lagrange multiplier γ

$$\mathcal{L}\left(\left[\hat{B}_r, \hat{D}_r \right]^T, \gamma \right) = \left\| \tilde{G}(z) - \hat{\chi} \begin{bmatrix} \hat{B}_r \\ \hat{D}_r \end{bmatrix} \right\|^2 + \gamma \left(\hat{\chi}_{1:} \begin{bmatrix} \hat{B}_r \\ \hat{D}_r \end{bmatrix} - \tilde{G}_1 \right) \tag{27}$$

Optimality conditions are:

$$\begin{gathered} \frac{\partial \mathcal{L}}{\partial \left[\hat{B}_r, \hat{D}_r \right]^T} \left(\left[\hat{B}_r, \hat{D}_r \right]^T, \gamma \right) = 2(\hat{\chi}^\dagger \hat{\chi}) \begin{bmatrix} \hat{B}_r \\ \hat{D}_r \end{bmatrix} - 2\hat{\chi}^T \tilde{G}(z) + \gamma \hat{\chi}_{1:} = 0 \\ \frac{\partial \mathcal{L}}{\partial \gamma} \left(\left[\hat{B}_r, \hat{D}_r \right]^T, \gamma \right) = \hat{\chi}_{1:} \begin{bmatrix} \hat{B}_r \\ \hat{D}_r \end{bmatrix} - \tilde{G}_1 = 0 \end{gathered} \tag{28}$$

Putting these into an augmented matrix gives the Karush-Kuhn-Tucker (KKT) [23] conditions:

$$\begin{bmatrix} 2(\hat{\chi}^\dagger \hat{\chi}) & \hat{\chi}_{1:}^T \\ \hat{\chi}_{1:} & 0 \end{bmatrix} \begin{bmatrix} \begin{bmatrix} \hat{B}_r \\ \hat{D}_r \end{bmatrix} \\ \gamma \end{bmatrix} = \begin{bmatrix} 2\hat{\chi}^T \tilde{G}(z) \\ \tilde{G}_1 \end{bmatrix} \tag{29}$$

If the KKT matrix is invertible, which is true for the ROM, gives new $\overline{\hat{B}_r}$ & $\overline{\hat{D}_r}$ matrices:

$$\begin{bmatrix} \begin{bmatrix} \overline{\hat{B}_r} \\ \overline{\hat{D}_r} \end{bmatrix} \\ \gamma \end{bmatrix} = \begin{bmatrix} 2(\hat{\chi}^\dagger \hat{\chi}) & \hat{\chi}_{1:}^T \\ \hat{\chi}_{1:} & 0 \end{bmatrix}^{-1} \begin{bmatrix} 2\hat{\chi}^T \tilde{G}(z) \\ \tilde{G}_1 \end{bmatrix} \tag{30}$$

Initial studies found that this was the most accurate method for steady-state correction, and hence is used here.

III.Results

ROMs have been generated for a NACA0012 airfoil at zero incidence and Mach numbers of $0.7, 0.75$, and 0.8 under gust excitations. The viscous mesh is 1001×201, with 701 cells on the airfoil surface, see Figure 1. Figure 2 show the steady pressure distribution for each test case.

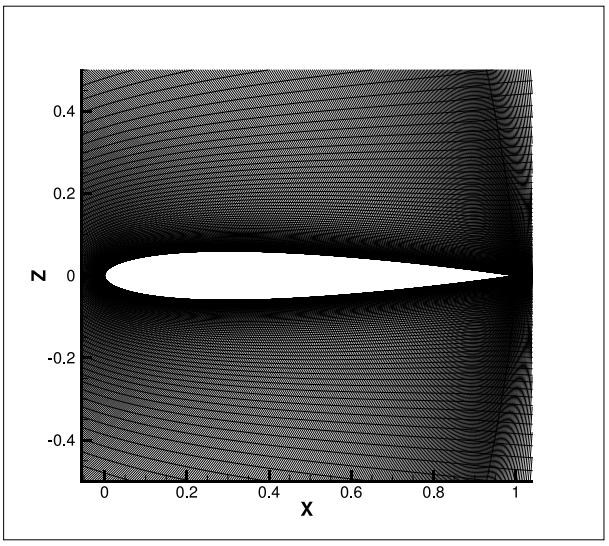

Figure 1. C grid magnified by a factor of 40

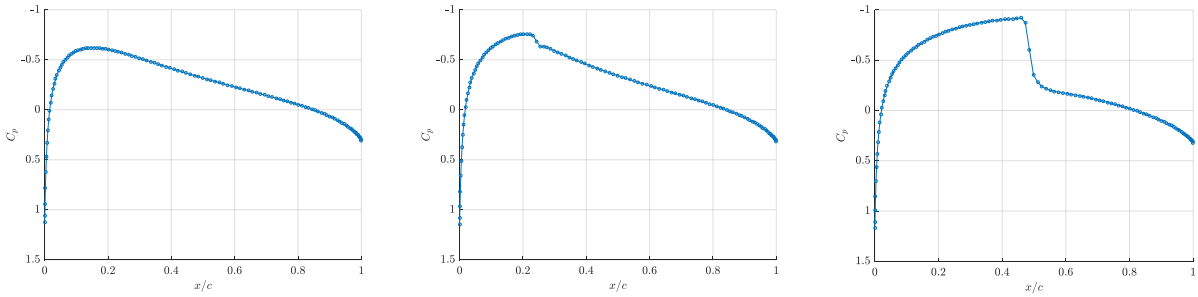

$\boldsymbol{M_\infty = 0.70}$ $\boldsymbol{M_\infty = 0.75}$ $\boldsymbol{M_\infty = 0.80}$

Figure 2. Steady pressure coefficient distributions

A. Reduced Order Models

ROMs, detailed in Table 1, were each generated using 81 discrete frequencies between 0 and π. Sampling period T changes the mapping to continuous frequencies, see Figure 3 with selection based on general knowledge of the dynamic system; here $T = 0.05/(2\pi)$ is chosen to capture the interesting system dynamics at lower frequencies, while also retaining some high frequency information. In general accuracy increases with ROM size, but at the expense of increased computational time. ROM sizes are kept as small as possible, whilst ensuring the system dynamics are

captured. A suitable size can be found be varying parameters, since once initial simulations are completed, ROM creation and testing is quick and computational inexpensive. It is not possible to estimate errors in the solution *apriori*.

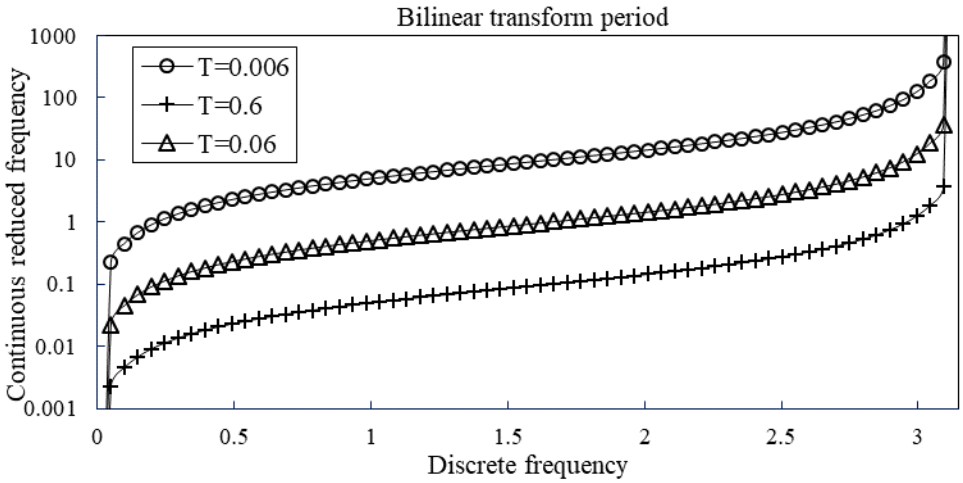

Figure 3. Impact of varying T

Table 1. ROMs

Test Case	Mach Number	ROM size	Number of Restarts
2	0.7	35	1
3	0.75	35	0
4	0.8	40	0

Figures 4 and 5 show the magnitude and phase of the ROMs, and eigenvalue plots showing the final ROMs are stable. Steady-state correction has been applied using the constrained least squared method. The frequency response is in good agreement with the LFD except that the ROM does not exhibit the oscillatory phase angle behavior seen for full-order simulations at the highest discrete frequencies. As the discrete frequency approaches π, from (14), the continuous frequency tends to infinity. At these high frequencies, the LFD code becomes ill-conditioned leading to oscillations. It is therefore important not to increase the ROM size too much to ensure oscillations at high frequencies do not compromise the model. This may mean losing some of the low frequency dynamics so a trade-off on model size must be undertaken to ensure the good models are created.

$M_\infty = 0.70$

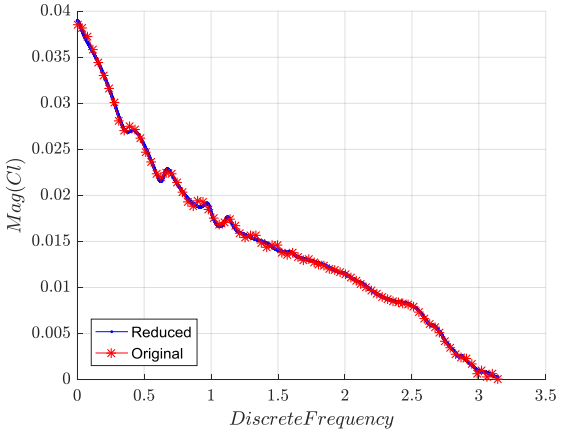

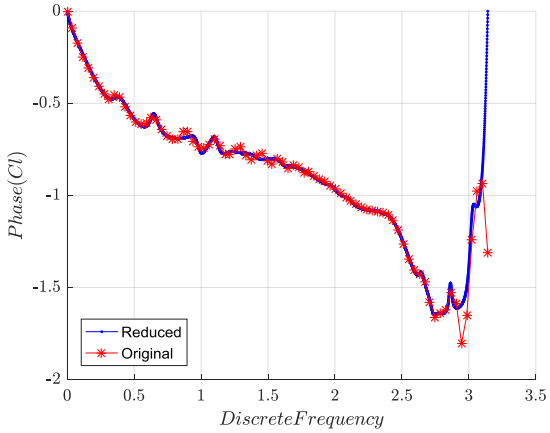

$M_\infty = 0.75$

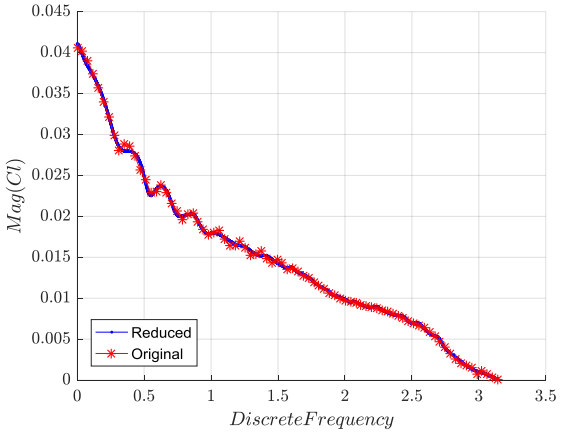

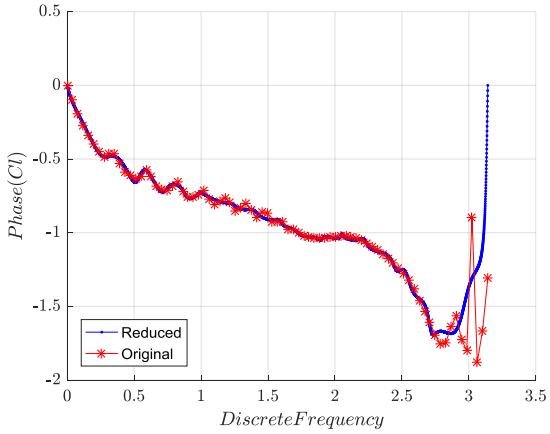

$M_\infty = 0.80$

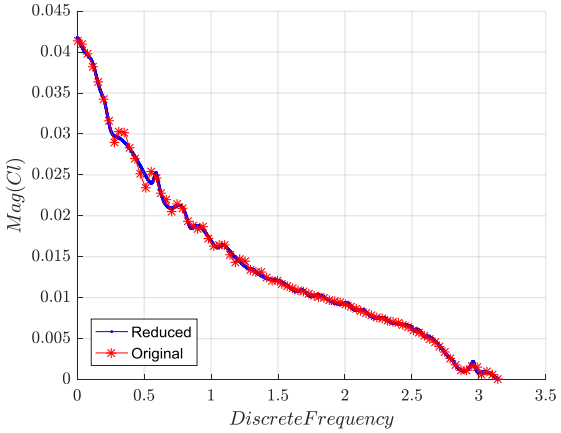

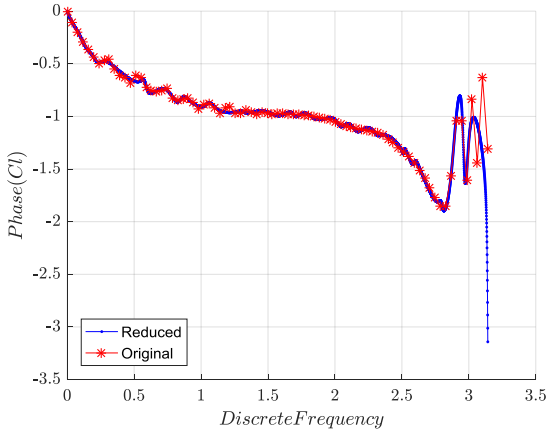

Figure 4. Frequency response magnitude and phase

$M_\infty = 0.70$

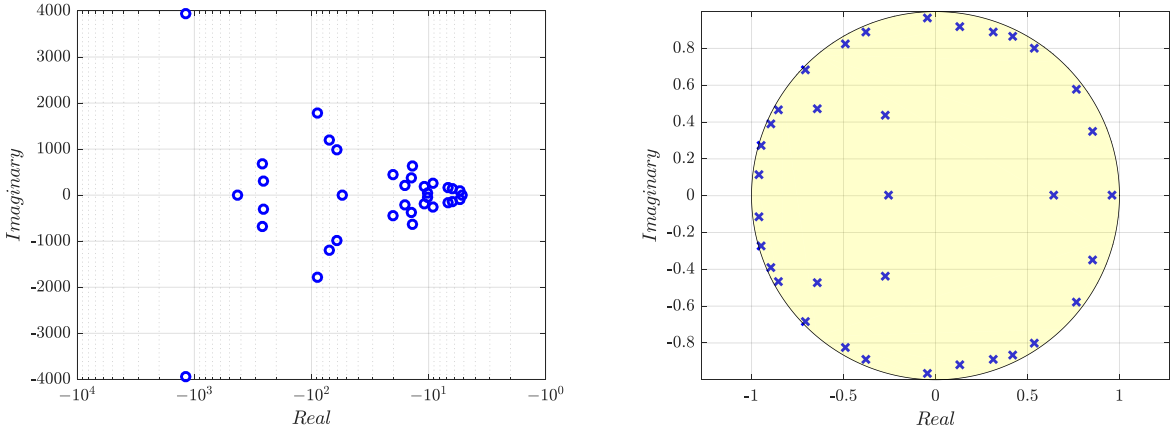

$M_\infty = 0.75$

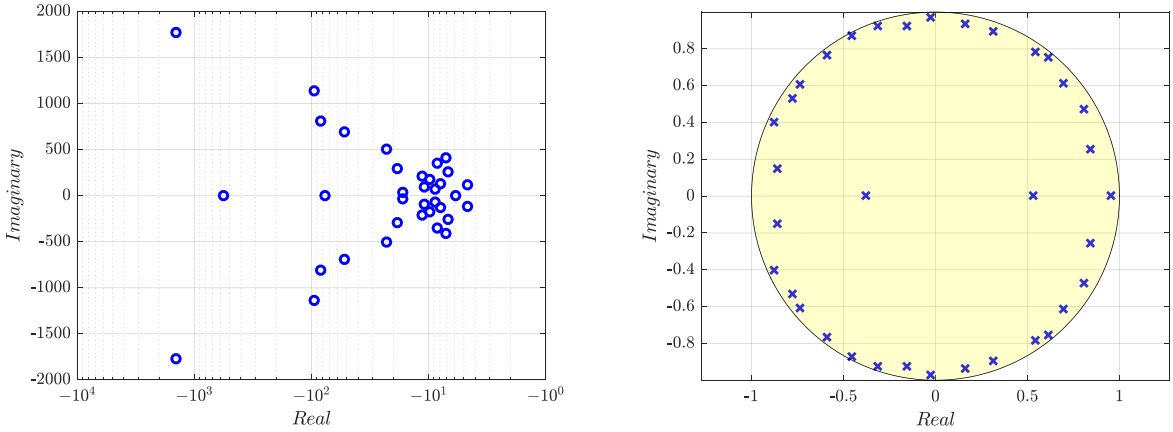

$M_\infty = 0.80$

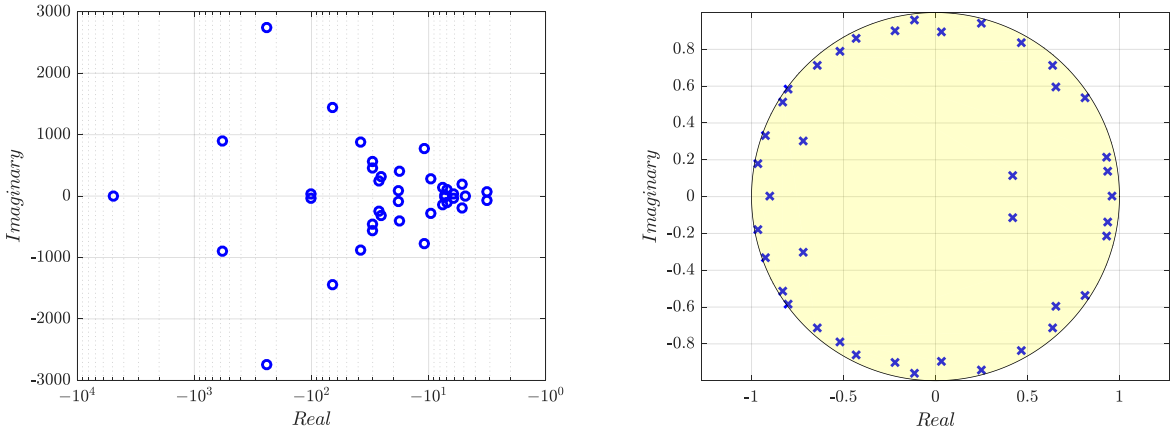

Figure 5. Eigenvalues: Continuous (left); Discrete (right)

B. ROM Testing

Predicted lift coefficients were compared to the full-order time-domain responses for 1-cosine gusts. The gust amplitude $v_{g_{max}}$ is set via the desired effective change in angle of attack:

$$v_{g_{max}} = \tan(\Delta\alpha_{eff}) \times u_{ref} \tag{31}$$

where u_{ref} is the free stream velocity and $\Delta\alpha_{eff} = 4^o$, see Table 2. In Figures 6-9, time is normalized with respect to the gust impact time with the airfoil leading edge. It can be seen that, for most gust profiles, the response from the ROM matches well with the full-order CFD simulation. Some of the dynamics as the gust settles to zero is also well captured. The peak lift coefficient value is predicted correctly, however at higher gust frequencies the models overpredict the maximum lift coefficient. The results at $M_\infty = 0.80$ exhibit some differences between the ROM and the full order results, particularly at the lowest gust frequency shown in Figure 6. This deficiency is worse at lower gust frequencies, as the gust progresses more slowly allowing more time for transient nonlinear responses to arise. It is known from Figure 2 that at $M_\infty = 0.80$ a strong shock wave is present on the airfoil surface and for the large gust length of $25c$, the nonlinear interaction between the shock and the boundary layer can affect the lift coefficient response. Since the ROMs are derived from LFD, they cannot capture nonlinearity. A ROM can only capture system dynamics if the CFD code from which it is derived can predict them.

Table 2. Gust cases

$\boldsymbol{\lambda}$ **(chords)**	$\boldsymbol{k_{red}}$	**Gust discrete frequency $\hat{\omega}$ for each Mach number**		
		0.7	**0.75**	**0.8**
25	0.126	0.468	0.500	0.532
10	0.314	1.074	1.136	1.195
3	1.047	2.208	2.263	2.311
1.5	2.094	2.648	2.680	2.708

$M_\infty = 0.70$

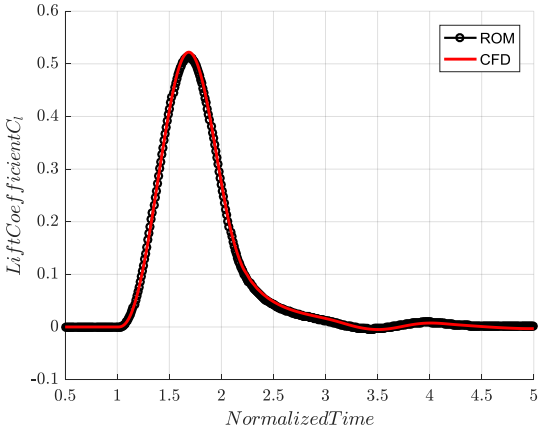

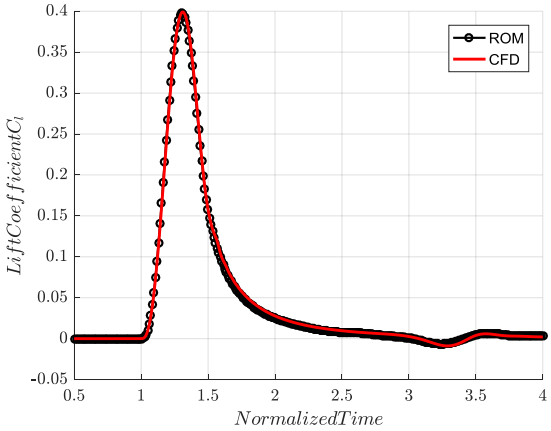

$M_\infty = 0.75$

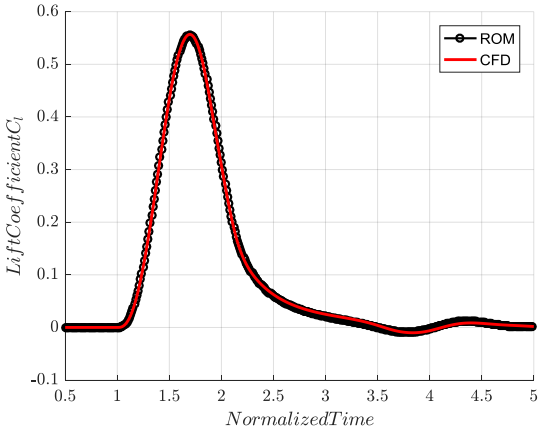

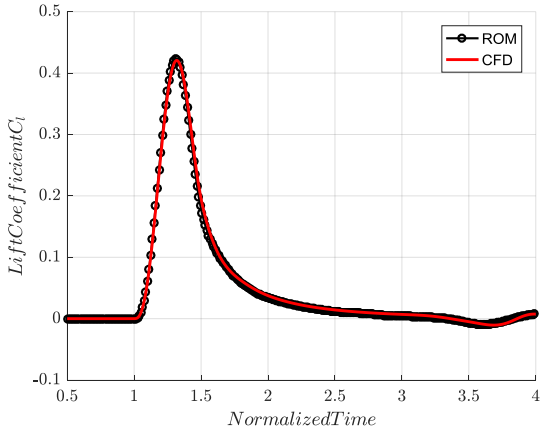

$M_\infty = 0.80$

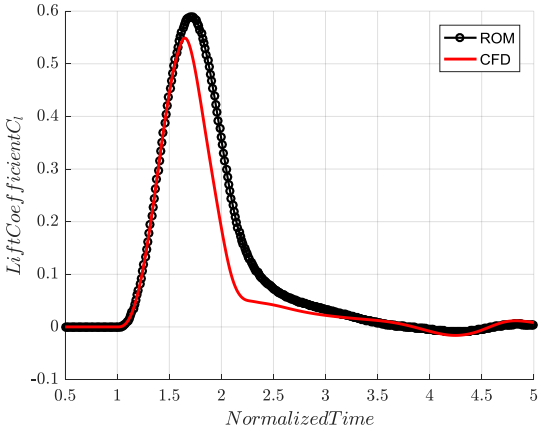

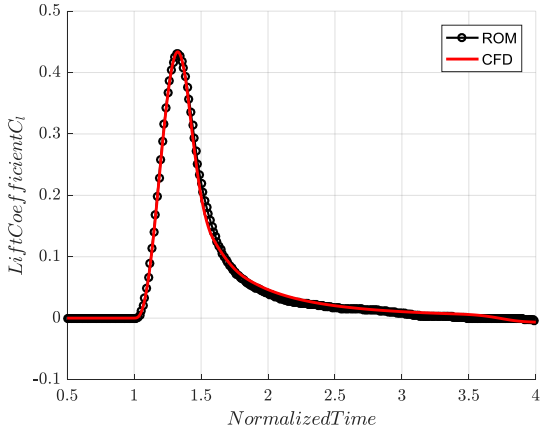

Figure 6. Cl response $\lambda = 25c$

Figure 7. Cl response $\lambda = 10c$

$M_\infty = 0.70$

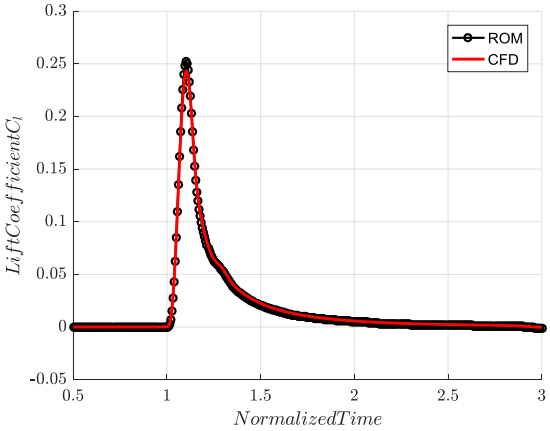

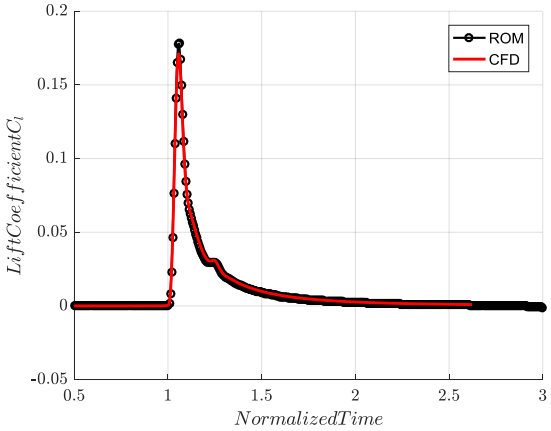

$M_\infty = 0.75$

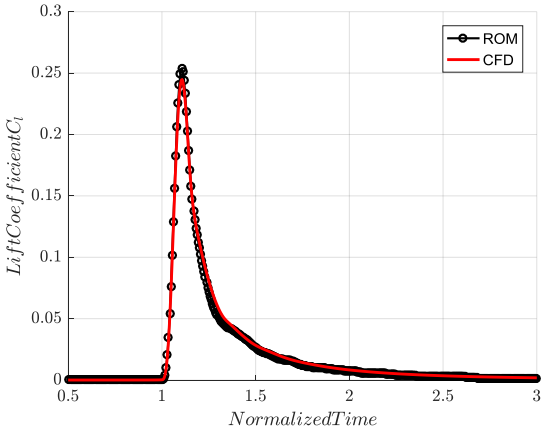

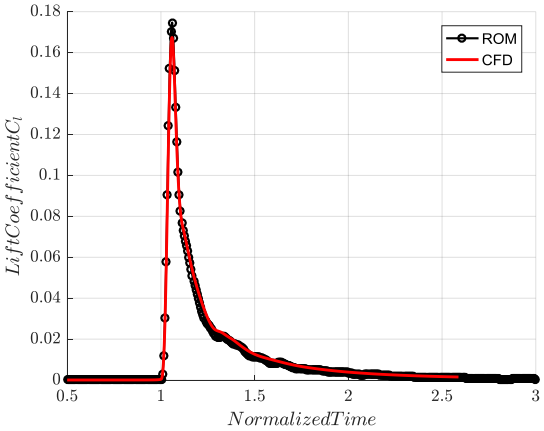

$M_\infty = 0.80$

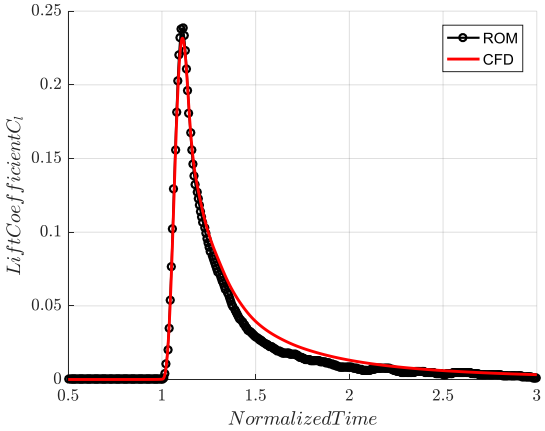

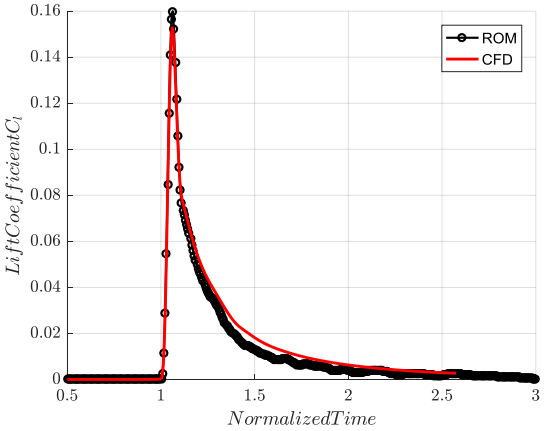

Figure 8. Cl response $\lambda = 3c$

Figure 9. Cl response $\lambda = 1.5c$

To understand how the methodology presented here fits within the wider context of gust modelling, results from the compressible Kussner function [15]

$$\psi(s) = 1.4 - 0563e^{-0.0542s} - 0.645e^{0.3125s} - 0.192e^{-1.474s} \tag{32}$$

at Mach 0.7 are compared to CFD results (from Figures 6-9). Here s is the reduced time, non-dimensionalized with respect to flow speed and airfoil chord. The comparisons shown in Figure 10 reveal that the Kussner function predicts a lower peak response at the highest gust length and that the response after the lift coefficient returns more quickly to the value before the gust encounter. This shows that linear theory is not capturing the full system dynamics in the CFD response, which the ROM is able to do. This suggests that the ROM shown in this paper has advantages compared to classical gust theories, while still being computationally inexpensive to run.

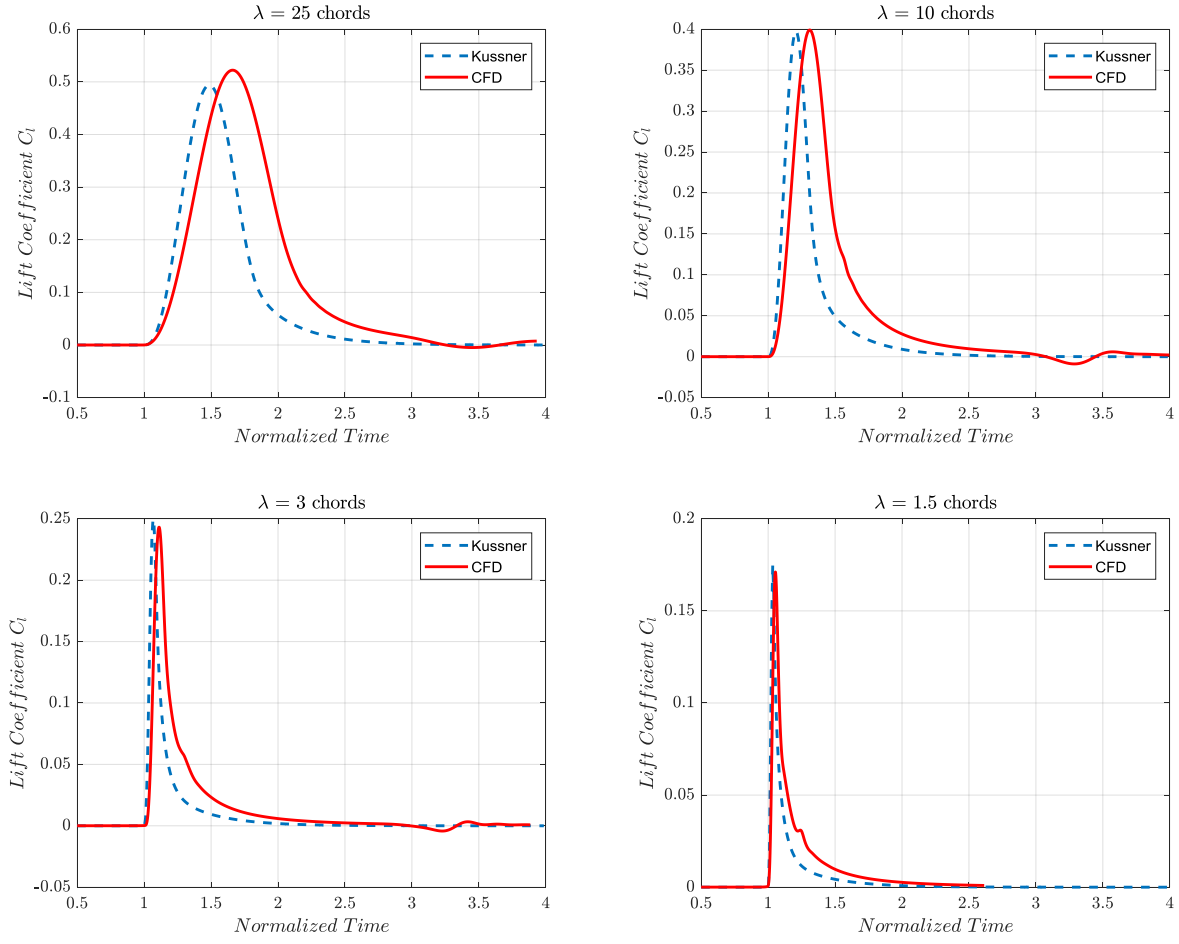

Figure 10. Kussner gust function versus ROM

IV. Conclusion

The ROM produced has the capacity to predict the output of the system to any input in a fraction of the time needed to run full order time domain simulations. Restarting has been shown to stabilize unstable reduced models by removing the unwanted unstable eigenvalues from the ROM and the steady state of the ROM has been successfully corrected to match the full order system via a constrained least squares problem. The advantage of the presented ROM is it does not require the formation and storage of large matrices. Future work will attempt to model nonlinearities arising from shockwaves and shock induced separation.

V.Acknowledgments

This research was co-funded by Innovative UK, within the Enhanced Fidelity Transonic Wing project.

VI.References

[1] S.-Y. Kung, K. Arun and B. R. D.V, "A new identification and model reduction algorithm via singular value decomposition," in *Proceedings of the 12th Asilomar conference on circuits, systems and computers*, 1978.

[2] J.-N. Juang and R. S. Pappa, "An eigensystem realization algorithm for modal parameter identification and model reduction," *Journal of guidance, control, and dynamics,* vol. 8, no. 5, pp. 620-627, 1985.

[3] L. Sirovich, "Turbulence and the dynamics of coherent structures, parts i–iii," *Quart. J. Appl. Math.,* vol. 45, pp. 561-590, 1987.

[4] K. Willcox and J. Peraire, "Balanced Model Reduction via the Proper Orthogonal Decomposition," *AIAA Journal,* vol. 40, no. 11, pp. 2323-2330, 2000.

[5] N. Falkiewicz and C. Cesnik, "Proper Orthogonal Decomposition for Reduced-Order Thermal Solution in Hypersonic Aerothermoelastic Simulations," *AIAA Journal,* vol. 49, no. 5, pp. 994-1009, doi: 10.2514/1.J050701 2011.

[6] D. J. Lucia, P. S. Beran and W. A. Silva, "Reduced-order modeling: new approaches for computational physics," *Progress in Aerospace Sciences,* vol. 40, no. 1, pp. 51-117, 2004, doi: 10.1016/j.paerosci.2003.12.001.

[7] K. Karhunen, *Ann. Acad. Sci. Fennicae, Ser. A1* , vol. 34, 1946.

[8] C. Wales, A. Gaitonde and D. Jones, "Reduced-Order Modeling of Gust Responses," *Journal of Aircraft,* vol. 54, pp. 1350-1363, 2017, doi: 10.2514/1.C033765.

[9] T. Skujins and C. C., "Reduced-Order Modeling of Unsteady Aerodynamics Across Multiple Mach Regimes," *Journal of Aircraft,* vol. 51, no. 6, pp. 1681-1704, 2014, doi: 10.2514/1.C032222.

[10] W. Zhang, J. Kou and Z. Wang, "Nonlinear Aerodynamic Reduced-Order Model for Limit-Cycle Oscillation and Flutter," *AIAA Journal,* vol. 54, no. 10, pp. 3302-3310, 2016, doi: 10.2514/1.J054951.

[11] D. Raveh, "CFD-Based Models of Aerodynamic Gust Response," *Journal of Aircraft,* vol. 44, p. 888–897, doi: 10.2514/1.25498. 2007.

[12] M. Gennaretti and F. Mastroddi, "Study of Reduced-Order Models for Gust-Response Analysis of Flexible Fixed Wings," *Journal of Aircraft,* vol. 51, p. 304–313, doi: 10.2514/1.C032222. 2014.

[13] T. McKelvey, H. Akçay and L. Ljung, "Subspace-based multivariable system identification from frequency response data," *Automatic Control, IEEE Transactions on,* vol. 41, no. 7, pp. 960-979, 1996.

[14] "Aerogust Project Final summary," Available from EC website, 2018.

[15] R. L. Bisplinghoff, A. Holt and R. L. Halfman, Aeroelasticity, New York: Dover Publications, 1996.